Inorg. Chem. **2002**, *41*, 1072–1078

Electrochemical, Spectroscopic, Structural, and Magnetic Characterization of the Reduced and Protonated α-Dawson Anions in $[Fe(\eta^5\text{-}C_5Me_5)_2]_5[HS_2Mo_{18}O_{62}]\cdot 3HCONMe_2\cdot 2Et_2O$ and $[NBu_4]_5[HS_2Mo_{18}O_{62}]\cdot 2H_2O$[1]

Suzy Juraja,[†] Truc Vu,[‡] Peter J. S. Richardt,[§] Alan M. Bond,*[,‡] Terence J. Cardwell,[†] John D. Cashion,[||] Gary D. Fallon,[‡] Georgii Lazarev,[‡] Boujemaa Moubaraki,[‡] Keith S. Murray,[‡] and Anthony G. Wedd[§]

Department of Chemistry, La Trobe University, Bundoora, Victoria 3083, Australia, School of Chemistry, P.O. Box 23, Monash University, Clayton, Victoria 3800, Australia, School of Chemistry, University of Melbourne, Parkville, Victoria 3052, Australia, and School of Physics & Materials Engineering, Monash University, Clayton, Victoria 3800, Australia

Received July 23, 2001

Reaction of excess $Fe(cp^*)_2$ ($cp^* = \eta^5\text{-}C_5Me_5$) dissolved in Et_2O with $[NHex_4]_4[S_2Mo_{18}O_{62}]$ in acetonitrile, followed by recrystallization of the precipitated solid from *N*,*N*′-dimethylformamide (DMF), leads to isolation of the complex $[Fe(cp^*)_2]_5[HS_2Mo_{18}O_{62}]\cdot 3DMF\cdot 2Et_2O$. The solid has been characterized by microanalysis, by voltammetric analysis, by ^1H NMR, diffuse reflectance infrared, EPR, and Mössbauer spectroscopies, and by temperature-dependent magnetic susceptibility measurements. The data are consistent with the presence of a paramagnetic $[Fe(cp^*)_2]^+$ cation and a diamagnetic two-electron-reduced $[HS_2Mo_{18}O_{62}]^{5-}$ anion. The related salt $[NBu_4]_5[HS_2Mo_{18}O_{62}]\cdot 2H_2O$ crystallizes in space group *C*2/*c* with $a = 25.1255(3)$ Å, $b = 15.4110(2)$ Å, $c = 35.8646(4)$ Å, $\beta = 105.9381(4)°$, $V = 13353.3(3)$ Å^3, and $Z = 4$. The (2 e$^-$, 1 H$^+$)-reduced anion exists as the α-Dawson isomer, and its structure may be compared with those of the oxidized and (4 e$^-$, 3 H$^+$)-reduced anions as they exist in $[NEt_4]_4[S_2Mo_{18}O_{62}]\cdot MeCN$ and $[NBu_4]_5[H_3S_2Mo_{18}O_{62}]\cdot 4MeCN$, respectively. Overall, the anion expands significantly upon the addition of two and then four electrons. However, the Mo···Mo distances along the bonds which connect the two equatorial belts *decrease* in the order 3.801, 3.780, and 3.736 Å, making these distances the shortest for the three inequivalent sets of corner-sharing octahedra in each anion. This is consistent with the two or four added electrons localizing essentially in molecular orbitals which are bondiing with respect to interactions between the belts.

Introduction

The versatile chemistry of polyoxometalate anions continues to attract interest.[2,3] One aspect concentrates on the versatile acidic and redox properties which can be tuned for catalysis and photochemistry.[4−7] For the particular case of the Dawson anion α-$[S_2Mo_{18}O_{62}]^{4-}$ an extensive series of reduction processes has been detected voltammetrically and photochemically.[8−14] Electrochemical syntheses of the simple (1 e$^-$)- and (2 e$^-$)-reduced forms $[S_2Mo_{18}O_{62}]^{5-}$ and $[S_2Mo_{18}O_{62}]^{6-}$ have been reported as well as those of the protonated (2 e$^-$, 1 H$^+$), (2 e$^-$, 2 H$^+$), (4 e$^-$, 2 H$^+$), and (4 e$^-$, 4 H$^+$) forms.[9,14] The use of phosphine reagents as

* To whom correspondence should be addressed. E-mail: Alan.Bond@sci.monash.edu.au. Fax: +61 3 99054597.
[†] La Trobe University.
[‡] School of Chemistry, Monash University.
[§] University of Melbourne.
[||] School of Physics & Materials Engineering, Monash University.

(1) Abbreviations: a, anodic, Bu, *n*-butyl; c, cathodic; *C*, concentration; CV, cyclic voltammetry; DMF, *N*,*N*′-dimethylformamide; δ, chemical or isomer shift; *E*, potential; $E_{1/2}^r$, reversible half-wave potential; E_f^o, reversible formal potential; ΔE_p, difference between peak potentials; equiv, equivalent; ΔE_Q, quadrupole splitting; Δ*H*, line width; *F*, Faraday's constant; $Fe(cp)_2$, ferrocene; $Fe(cp^*)_2$, decamethylferrocene; G, gauss; Hex, *n*-hexyl; *i*, current; i_L, limiting current; i_p, peak current; Λ_e, equivalent conductivity; Λ_o, conductivity at infinite dilution; *M*, molar concentration; μ_B, Bohr magneton; μ_{eff}, effective magnetic moment; *n*, number of electrons transferred per molecule; N_r, rotation rate (min^{-1}); phen, *o*-phenanthroline; RDEV, rotating disk electrode voltammetry; *T*, temperature; TIP, temperature-independent paramagnetic susceptibility; Θ, Curie−Weiss constant; *ν*, scan rate; *ω*, rotation rate (s^{-1}); χ_m, molar magnetic susceptibility.

(2) Pope, M. T. *Heteropoly and Isopoly Oxometalates*; Springer-Verlag: Berlin, 1983.

10.1021/ic010780s CCC: $22.00 © 2002 American Chemical Society
Published on Web 02/08/2002

reductants[15] also allows access to some of the above species,[11] as well as to a salt characterized by X-ray crystallography as containing a (4 e^-, 3 H^+)-reduced anion.[16]

In the present study, decamethylferrocene $Fe(cp^*)_2$ was employed as a clean chemical reductant, using rotating disk electrode voltammetry to monitor the redox and protonation levels of products in solution. The salt $[Fe(cp^*)_2]_5[HS_2Mo_{18}O_{62}]\cdot 3DMF\cdot 2Et_2O$ has been characterized in detail and shown to contain paramagnetic $[Fe(cp^*)_2]^+$ cations and a diamagnetic (2 e^-, 1 H^+)-reduced $[HS_2Mo_{18}O_{62}]^{5-}$ anion. Magnetic interactions in such species are of much current interest,[17,18] although they appear to be very weak in this salt and in related species.[17,18] The properties of the salt $[NBu_4]_5[HS_2Mo_{18}O_{62}]\cdot 2H_2O$ have also been examined, and its crystal structure has been determined. This allows a detailed comparison of the structure of the α-Dawson anion in this (2 e^-, 1 H^+)-reduced form with those in the oxidized and (4 e^-, 3 H^+)-reduced forms.[8,16]

Experimental Section

Reagents. DMF (AUSPEP, AR grade), diethyl ether (BDH, AR grade), acetonitrile (Mallinckrodt, Biolab Scientific Pty Ltd., ChromHPLC grade), and $Fe(cp^*)_2$ and $Fe(cp)_2$ (Strem Chemicals) were all used as received.

Synthesis. The syntheses of α-$[NHex_4]_4[S_2Mo_{18}O_{62}]$, $[NBu_4]_5[S_2Mo_{18}O_{62}]$, and $[NBu_4]_5[HS_2Mo_{18}O_{62}]$ employed literature procedures.[14]

$[Fe(cp^*)_2]PF_6$. A solution of $Fe(cp^*)_2$ (5 mM) in MeCN (0.1 M NBu_4PF_6) was oxidized at 0 mV vs Ag^+/Ag by controlled potential electrolysis until the faradaic current decayed to zero (about 20 min). Coulometry confirmed the transfer of 0.95(5) electron per molecule. The solid product formed after refrigeration overnight at 4 °C was washed with water and ethanol and dried under vacuum.

$[Fe(cp^*)_2]_5[HS_2Mo_{18}O_{62}]\cdot 3DMF\cdot 2Et2O$. A solution of $[Fe(cp^*)_2]$ in Et_2O (0.6 mM, 20 mL) was added dropwise to a solution of $[NHex_4]_4[S_2Mo_{18}O_{62}]$ in MeCN (0.2 mM, 30 mL), and the blue precipitate was filtered off. The filtrate was left to stand for a day, and a second crop was obtained. The solids were recrystallized from DMF. Yield: 10%. Anal. Found: C, 28.74; H, 3.86; Fe, 5.84; Mo, 36.22; N, 0.86; S, 1.39%. $C_{117}H_{192}Fe_5Mo_{18}N_3O_{67}S_2$ requires C, 29.38; H, 4.05; Fe, 5.84; Mo, 36.10; N, 0.88; S, 1.34%. ^{1}H NMR (Me_2SO-d_6): 7.95 (s, *H*CO, 3 H), 2.91−2.75 (m, H_3CN, 9 H), 1.31 (t, H_3CH_2C, 12 H) ppm.

Limiting rotating disk electrode voltammetry (RDEV) currents of $[Fe(cp^*)_2]PF_6$ and $[NBu_4]_5[HS_2Mo_{18}O_{62}]$ in MeCN/H_2O (95:5 v/v; NBu_4PF_6, 0.1 M; $HClO_4$, 0.1 M) were calibrated and applied to analysis of the cation:anion ratio in $[Fe(cp^*)_2]_5[HS_2Mo_{18}O_{62}]\cdot 3DMF\cdot 2Et_2O$ dissolved in the same medium (see Figures 1 and 3). Anal. Found: $[Fe(cp^*)_2]^+$, 34.1(1); $S_2Mo_{18}O_{62}$, 58(2)%. A 5:1 ratio requires $[Fe(cp^*)_2]^+$, 34.1; $S_2Mo_{18}O_{62}$, 56.3%.

Physical and Analytical Techniques. Fe and Mo analyses employed standard atomic absorption spectrometric techniques. Other elemental microanalysis was performed by the Analytical Laboratory, University of Otago, Dunedin, New Zealand. Infrared spectra were acquired in the diffuse reflectance mode on powdered mixtures of sample in KBr using a Perkin-Elmer Fourier transform infrared spectrometer (1720X) equipped with an Epson PC AX2 computer. Conductivity measurements utilized an Activon (model PTI-10) portable digital conductivity (μS cm^{-1})/temperature (°C) meter. The cell constant was determined as 0.8744 with a standard 10^{-2} M aqueous KCl solution at 20 °C whose specific conductance (κ) was assumed to be 1.278×10^{-3} Ω^{-1} cm^{-1}.[19] Conductivities were measured as a function of concentration at 20 °C, enabling application of the Onsager law ($\Lambda_o - \Lambda_e = (A + \omega B\Lambda_o)C^{1/2}$).[20] The term $A + \omega B\Lambda_o$ depends on the charges of the ions concerned, ω is related to ionic mobilities, Λ_o is the conductivity at infinite dilution, Λ_e is the equivalent conductivity, and C is the equivalent concentration.

X-Band EPR Spectra. ESR measurements were made with a Bruker ESP-380 spectrometer operating at 6 K. A gain of 6.3×10^3 and modulation amplitude of 6.3 G were used. The g values were estimated via calibration with DPPH.[21]

Electrochemistry. All voltammograms were acquired at 22 °C using a Cypress Systems model CS-1090 computer-controlled electroanalytical system in the staircase mode. Rotating-disk electrode voltammetry employed a variable-speed rotator (Metrohm 628-10). Solvents used in electrochemical experiments were degassed with dinitrogen that had been presaturated with solvent. A standard three-electrode electrochemical cell arrangement was employed. A glassy carbon disk (d = 3.0 mm) was used as the working electrode. The counter electrode was a platinum wire. Ag^+/Ag (MeCN; $AgNO_3$, 0.01 M; NBu_4PF_6, 0.1 M) was used as the reference electrode. Controlled potential electrolysis was carried out using a Bioanalytical System model 100 electrochemical analyzer. The electrolysis cell contained two Pt baskets which served as the working and counter electrodes. The working electrode was arranged symmetrically inside the counter electrode and separated

(3) Pope, M. T.; Müller, A. *Polyoxometalates: From Platonic Solids to Antiretroviral Activity*; Kluwer Academic: Dordecht, The Netherlands, 1994.
(4) Hill, C. L.; Prosser-McCartha, C. M. *Coord. Chem. Rev.* **1995**, *143*, 407−455.
(5) Kozhevnilov, I. V. *Chem. Rev.* **1998**, *98*, 171−198.
(6) Neumann, R. *Prog. Inorg. Chem.* **1998**, *47*, 317−370.
(7) Mizuno, N.; Misono, M. *Chem. Rev.* **1998**, *98*, 199−217.
(8) Hori, T.; Tamada, O.; Himeno, S. *J. Chem. Soc., Dalton Trans.* **1989**, 1491−1495.
(9) Way, D. M.; Bond, A. M.; Wedd, A. G. *Inorg. Chem.* **1997**, *36*, 2826−2833 and refs therein.
(10) Bond, A. M.; Way, D. M.; Wedd, A. G.; Compton, R. G.; Booth, J.; Eklund, J. C. *Inorg. Chem.* **1995**, *34*, 3378−3384.
(11) Bond, A. M.; Eklund, J. C.; Tedesco, V.; Vu, T.;. Wedd, A. G. *Inorg. Chem.* **1998**, *37*, 2366−2372.
(12) (a) Cartié, B. *J. Chem. Res., Synop.* **1988**, 290−291. (b) Himeno, S.; Osakai, T.; Saito, A.; Hori, T. *Bull. Chem. Soc. Jpn.* **1992**, *65*, 799−804. (c) Osakai, T.; Himeno, S.; Saito, A. *J. Electroanal. Chem.* **1992**, *332*, 169−182. (d) Himeno, S.; Osakai, T.; Saito, A.; Maeda, K.; Hori, T. *J. Electroanal. Chem.* **1992**, *337*, 371−374. (e) Himeno, S.; Maeda, K.; Osakai, T.; Saito, A.; Hori, T. *Bull. Chem. Soc. Jpn.* **1993**, *66*, 109−113.
(13) Eklund, J. C.; Bond, A. M.; Humphrey, D. G.; Lazarev, G.; Vu, T.; Wedd, A. G.; Wolfbauer, G. *J. Chem. Soc., Dalton Trans.* **2000**, 4373−4378.
(14) Way, D. M.; Cooper, J. B.; Sadek, M.; Vu, T.; Mahon, P. J.; Bond, A. M.; Brownlee, R. C.; Wedd, A. G. *Inorg. Chem.* **1997**, *36*, 4227−4233. Erratum. *Inorg. Chem.* **1998**, *37*, 604 and references therein.
(15) Kawafune, I.; Matsubayashi, G. *Inorg. Chim. Acta* **1991**, *188*, 33−39.
(16) Neier, R.; Trojanowski, C.; Mattes, R. *J. Chem. Soc., Dalton Trans.* **1995**, 2521−2828.
(17) Ouahab, L.; Bencharif, M.; Mhanni, A.; Pelloquin, D.; Halet, J.-F.; Pena, O.; Padrou, J.; Grandjean, D.; Garrigou-Lagrange, C.; Amsell, J.; Delhaes, P. *Chem. Mater.* **1992**, *4*, 666−674.
(18) Le Magueres, P.; Ouahab, L.; Golhen, S.; Grandjean, D.; Pena, O.; Jegaden, J.-C.; Gomez-Garcia, C. J.; Delhaes, P. *Inorg. Chem.* **1994**, *33*, 5180−5187. Coronado, E.; Gomez-Garcia, C. J. *Chem. Rev.* **1998**, *98*, 273−296. Ouahab, L. *Chem. Mater.* **1997**, *9*, 1909−1926.
(19) Christian, G. D.; O'Reilly, J. E. *Instrumental Analysis*; Allyn and Bacon: Newton, MA, 1986; p 125.
(20) Geary, W. L. *Coord. Chem. Rev.* **1971**, *7*, 81−122.
(21) Wertz, J. E.; Bolton, J. R. *Electron Spin Resonance. Elementary Theory and Practical Applications*; McGraw-Hill: New York, 1972; p 464.

by a glass cylinder with a porous glass frit in the base.[22] The reference electrode was positioned as close as possible to the working electrode to maximize the uniformity of potential over its surface.

Magnetic Susceptibility. Variable-temperature susceptibility measurements (300−4.2 K) were performed on powdered samples at a field strength of 10000 G (1 T) using a Quantum Design MPMS Squid magnetometer. The calibration of the instrument was checked against $CuSO_4 \cdot 5H_2O$ and a standard palladium sample supplied by the manufacturer. Samples were enclosed in gelatine capsules suspended in the middle of a plastic drinking straw, which was rigidly fixed to the end of the sample rod. The magnetic susceptibilities were corrected for diamagnetic contributions (χ_{dia}) for the anion and the organometallic cation by use of Pascal's tables. For $[Fe(cp^*)_2]_5[HS_2Mo_{18}O_{62}] \cdot 3DMF \cdot 2Et_2O$, $\chi_{dia} = -2089 \times 10^{-6}$ cm^3 mol^{-1}, which is similar in magnitude to values used recently for salts of one-electron-reduced anions $[PMo_{12}O_{40}]^{4-}$ and $[SiMo_{12}O_{40}]^{5-}$.[17,18] In these studies, it was assumed that deviations from linearity in the χ_m^{-1} versus temperature plots (and corresponding variation of $\chi_m T$ (or μ_{eff}) with T) were due to a temperature-independent paramagnetic (TIP) term on the cluster. This TIP term was large (approximately 1000×10^{-6} cm^3 mol^{-1}) and similar in size to the χ_{dia} value.[17,18] It was subtracted to leave a linear χ_m^{-1} versus T dependence. The TIP term for $[Fe(cp^*)_2]_5[HS_2Mo_{18}O_{62}] \cdot 3DMF \cdot 2Et_2O$ is 1450×10^{-6} cm^3 mol^{-1}.

Mössbauer Spectroscopy. A standard electromechanical transducer operating in a symmetrical constant-acceleration mode was used to obtain Mössbauer spectra at room temperature (20 °C). The sample was crushed in a mortar and pestle, and 100 mg was loaded into a Perspex absorber holder and sealed. Data were collected with an LS1-based 1000-channel multichannel analyzer which decreases to 500 channels after folding. Velocity calibration and isomer shift reference were made with respect to α-Fe (iron foil) at room temperature. Spectra were fitted with a Lorentzian line shape using least-squares minimization. They could be fitted either as a singlet or as a quadrupole doublet in which the quadrupole splitting, ΔE_Q, is very small. The isomer shift, δ, is the same for both fits. Fit a: singlet, $\delta = 0.43(1)$ mm s^{-1}, line width 0.58(1) mm s^{-1} (full width at half-maximum height). Fit b: doublet, $\delta = 0.43(1)$ mm s^{-1}; line width 0.50(1) mm s^{-1}, $\Delta E_Q = 0.19(1)$ mm s^{-1}. Fit b is favored marginally from goodness of fit data.

X-ray Crystallography. Dark blue crystals of $[NBu_4]_5[HS_2Mo_{18}O_{62}] \cdot 2H_2O$ suitable for a single-crystal X-ray structure determination were obtained by diffusion of Et_2O into a MeCN solution of the compound. A blue tabular crystal of approximate dimensions $0.21 \times 0.16 \times 0.09$ mm was mounted onto a glass fiber. X-ray measurements for this compound were made at 173 ± 2 K, on a Nonius Kappa CCD diffractometer with graphite-monochromated Mo Kα radiation. The structure was solved and expanded by Fourier techniques.[23] All non-hydrogen atoms were refined anisotropically except carbon, which was refined isotropically. Hydrogen atoms were included but not refined, except those on disordered carbon atoms, the anion, and the waters of crystallization, which were not included. Crystallographic data are presented in Table 1 and Tables S1−S4 in the Supporting Information.

(22) Fry, A. J. *Synthetic Organic Electrochemistry*; Wiley: New York, 1989.

(23) Beurskens, P. T.; Admiraal, G.;. Beurskens, G.; Bosman, W. P.; de Gelder, R.; Israel, R.; Smits, J. M. M. *The DIRDIF-94 Program System*; Technical Report of the Crystallographic Laboratory; University of Nijmegen: Nijmegen, The Netherlands, 1994.

Table 1. Crystallographic Data for $[NBu_4]_5[HS_2Mo_{18}O_{62}] \cdot 2H_2O$

empirical formula	$C_{80}H_{185}Mo_{18}N_5O_{64}S_2$	T, °C	−100 ± 2
		D_{calcd}, g cm^{-3}	2.01
fw	4032.4	F_{000}	8000
color, habit	blue, tabular	μ(Mo Kα), cm^{-1}	17.43
size, mm	0.21 × 0.16 × 0.09	diffractometer	Nonius Kappa CCD
		$2\theta_{max}$, deg	54.2
cryst syst	monoclinic	no. of reflns	total, 89527
lattice type	C-centered		unique, 14633 ($R_{int} = 0.045$)
space group	$C2/c$ (no. 15)		
a, Å	25.1255(3)	no. of obsd reflns	9796
b, Å	15.4110(2)	($I > 2.0\sigma(I)$)	
c, Å	35.8646(4)	no. of variables	578
β, deg	105.9381(4)	no. of reflns/param	16.95
V, Å^3	13353.3(3)	residuals R, R_w	0.041, 0.052
Z	4	function minimized	$\sum w(\|F_o\| - \|F_c\|)^2$

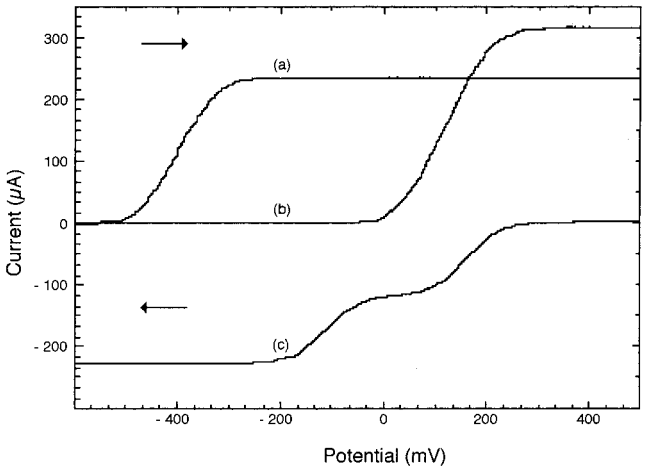

Figure 1. Steady-state rotated disk electrode voltammograms of (a) $Fe(cp^*)_2$ (2.6 mM), (b) $Fe(cp)_2$ (3.5 mM), and (c) $[NHex_4]_4[S_2Mo_{18}O_{62}]$ (2.6 mM) in MeCN (NBu_4PF_6, 0.1 M). $\nu = 0.1$ V s^{-1}; $\omega = 40$ s^{-1}. The reference electrode is Ag/Ag^+ (MeCN; $AgNO_3$, 0.01 M; NBu_4PF_6, 0.1 M).

Results and Discussion

Voltammetric Monitoring of the Reduction of $[S_2Mo_{18}O_{62}]^{4-}$ by $Fe(cp^*)_2$. RDEV established the reversible formal potentials E_f^o for the reduction of $[S_2Mo_{18}O_{62}]^{4-}$ and oxidation of $Fe(cp^*)_2$. Assuming that they are equivalent to the reversible half-wave potentials $E_{1/2}^r$, the thermodynamic basis of the reaction can be addressed. In addition, the position of zero current allows the redox level of $[S_2Mo_{18}O_{62}]^{4-}$ to be monitored.

Figure 1 shows the rotating disk voltammograms in MeCN (NBu_4PF_6, 0.1 M) for oxidation of $Fe(cp^*)_2$ and $Fe(cp)_2$ (used for reference potential calibration) and for the reduction of $[S_2Mo_{18}O_{62}]^{4-}$ (first two one-electron processes only, $[S_2Mo_{18}O_{62}]^{4-/5-}$ and $[S_2Mo_{18}O_{62}]^{5-/6-}$). It is apparent from the reversible potential data extracted from Figure 1 that $Fe(cp^*)_2$ is thermodynamically capable of reducing $[S_2Mo_{18}O_{62}]^{4-}$ to the (2 e$^-$)-reduced redox level:

$$2Fe(cp^*)_2 + [S_2Mo_{18}O_{62}]^{4-} \rightarrow 2[Fe(cp^*)_2]^+ + [S_2Mo_{18}O_{62}]^{6-} \quad (1)$$

Figure 2 shows the effect of titration of $[S_2Mo_{18}O_{62}]^{4-}$ into a 2.0 mM solution of $Fe(cp^*)_2$. The position of zero current indicates the progressive oxidation of $Fe(cp^*)_2$ and a commensurate increase in current intensity for the

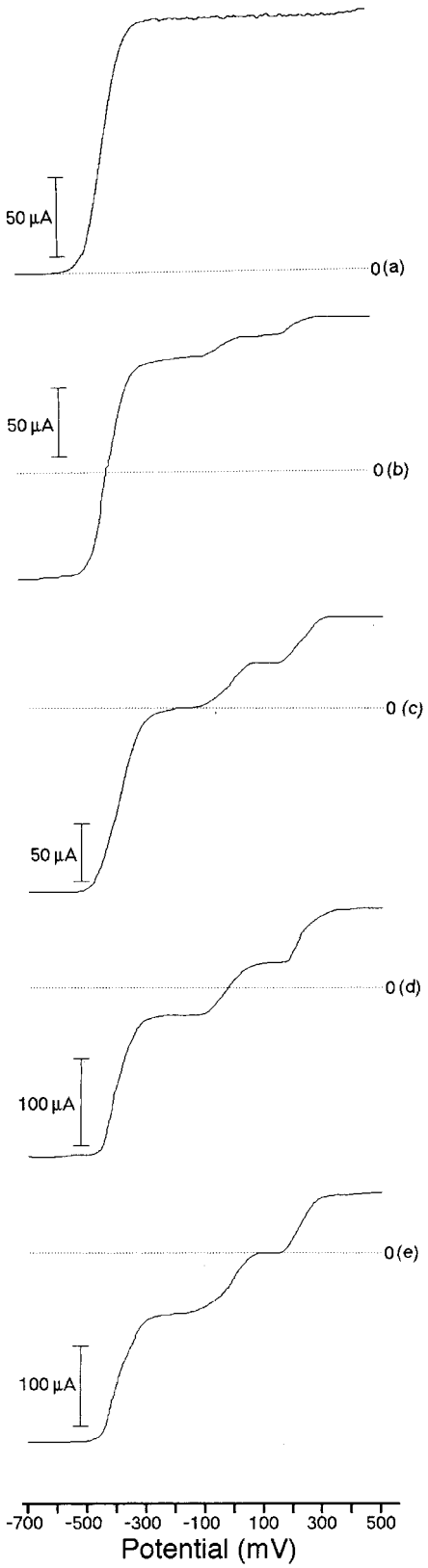

Figure 2. Steady-state rotated disk electrode voltammograms of $Fe(cp^*)_2$ in MeCN (2 mM; NBu_4PF_6, 0.1 M) as a function of $[NHex_4]_4[S_2Mo_{18}O_{62}]$: (a) 0.0 mM; (b) 0.5 mM; (c) 1.0 mM; (d) 1.5 mM; (e) 2.0 mM. $\nu = 0.01$ V s^{-1}; $\omega = 40$ s^{-1}. The position of zero current is indicated by a dotted line. The reference electrode is Ag/Ag^+ (MeCN; $AgNO_3$, 0.01 M; NBu_4PF_6, 0.1 M).

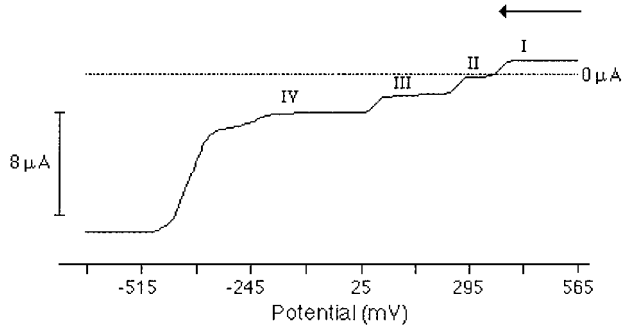

Figure 3. Steady-state rotated disk electrode voltammogram of $[Fe(cp^*)_2]_5[HS_2Mo_{18}O_{62}]\cdot 3DMF\cdot 2Et_2O$ in $MeCN/H_2O$ (95:5 v/v; NBu_4PF_6, 0.1 M; $HClO_4$, 0.1 M). $\nu = 0.1$ V s^{-1}; $\omega = 40$ s^{-1}. The reference electrode is Ag/Ag^+ (MeCN; $AgNO_3$, 0.01 M; NBu_4PF_6, 0.1 M).

$[S_2Mo_{18}O_{62}]^{4-/5-}$ and $[S_2Mo_{18}O_{62}]^{5-/6-}$ processes. At an $Fe(cp^*)_2$:$S_2Mo_{18}O_{62}$ concentration ratio of 2:1, the position of zero current lies exactly between the $Fe(cp^*)_2^{0/-}$ and $[S_2Mo_{18}O_{62}]^{5-/6-}$ processes (Figure 2c), in complete accord with eq 1. In contrast, at a concentration ratio of 1:1 (Figure 2e), the position of zero current lies midway between the $[S_2Mo_{18}O_{62}]^{4-/5-}$ (oxidation) and $[S_2Mo_{18}O_{62}]^{5-/6-}$ (reduction) processes, as predicted from the relative $E_{1/2}{}^r$ values indicated by Figure 1:

$$Fe(cp^*)_2 + [S_2Mo_{18}O_{62}]^{4-} \rightarrow [Fe(cp^*)_2]^+ + [S_2Mo_{18}O_{62}]^{5-} \quad (2)$$

In confirmation, titration of solid (1 e^-)-reduced $[NBu_4]_5[S_2Mo_{18}O_{62}]$ into $Fe(cp^*)_2$ solution required one equiv of $[S_2Mo_{18}O_{64}]^{5-}$ according to the reaction

$$Fe(cp^*)_2 + [S_2Mo_{18}O_{62}]^{5-} \rightarrow [Fe(cp^*)_2]^+ + [S_2Mo_{18}O_{62}]^{6-} \quad (3)$$

Characterization of $[Fe(cp^*)_2]_5[HS_2Mo_{18}O_{62}]\cdot 3DMF\cdot 2Et_2O$. The voltammetric monitoring of Figure 2 confirmed that $Fe(cp^*)_2$ acts as a very clean one-electron reducing reagent in this system. Synthesis at the stoichiometry of eq 1 in DMF/Et_2O, or with an excess of $Fe(cp^*)_2$, led to precipitation of $[Fe(cp^*)_2]_5[HS_2Mo_{18}O_{62}]\cdot 3DMF\cdot 2Et_2O$ as the least soluble salt. ^1H NMR confirmed the presence of DMF and Et_2O as solvents of crystallization (see the Experimental Section), despite line broadening due to the presence of paramagnetic $[Fe(cp^*)_2]^+$ cations. While sparingly soluble in DMF and Me_2SO, solubility is increased in the presence of the electrolyte NBu_4PF_6. A solution in $MeCN/H_2O$ (95:5 v/v; NBu_4PF_6, 0.1 M) containing $HClO_4$ (0.1 M) showed the presence of four 2 e^- processes, I−IV (Figure 3).[14] The position of zero current confirms the presence of a (2 e^-)-reduced form of $[S_2Mo_{18}O_{62}]^{4-}$. The additional reduction process in Figure 3 is assigned to the presence of $[Fe(cp^*)_2]^+$ (cf. Figure 1). Calibration of limiting currents confirmed a cation:anion ratio of 5:1 (see the Experimental Section).

Extensive conductance data are available for electrolytes dissolved in DMF.[20,24−27] Equivalent conductivities were

(24) Vogel, A. I. *A Text-Book of Quanlitative Inorganic Analysis including Elementary Instrumental Analysis*; Longman Group Ltd.: London, 1961.

Table 2. Conductance Data in DMF[a]

compound	Λ_o	slope	electrolyte type
$[Ni(phen)_{3}](PF_6)_2$	167	2.7×10^2	1:2
$[NBu_4]_3[PMo_{12}O_{40}]$	275	5.5×10^3	1:3
$[NHex_4]_4[S_2Mo_{18}O_{62}]$	369	9.0×10^3	1:4
$[NBu_4]_5[HS_2Mo_{18}O_{62}]$	607	3.2×10^5	1:5
$[Fe(cp^*)_2]_5[HS_2Mo_{18}O_{62}](DMF)_3(Et_2O)_2$	591	3.0×10^5	1:5

[a] Estimated from plots of Λ_e vs $C^{1/2}$ and $\Lambda_o - \Lambda_e$ vs $C^{1/2}$ plots (Table S5).

estimated for $[Fe(cp^*)_2]_5[HS_2Mo_{18}O_{62}]\cdot 3DMF\cdot 2Et_2O$ and a range of electrolytes (Tables S5 and 2). It is apparent that the former is a 5:1 electrolyte, consistent with its stoichiometry.

EPR and Mössbauer Spectroscopies. The EPR spectrum of powdered $[Fe(cp^*)_2]_5[HS_2Mo_{18}O_{62}]\cdot 3DMF\cdot 2Et_2O$ can be observed at $T < 26$ K (Figure S1). Parameters $g_{\parallel} = 3.89$ (line width $\Delta H = 400$ G) and $g_{\perp} = 1.32$ ($\Delta H = 1800$ G) are consistent with the presence of low-spin Fe^{III} ($S = {}^1/_2$, ^2E_g ground state) centers from the $[Fe(cp^*)_2]^+$ cations.[18] No EPR signal was observed from the polyoxometalate anion. EPR signals have been detected previously for (1 e^-)- and (3 e^-)-reduced forms of $[S_2Mo_{18}O_{62}]^{4-}$ but not for a (2 e^-)-reduced form.[13]

The room-temperature Mössbauer spectrum consists of a single line which could be fitted as either a singlet or a quadrupole doublet in which the quadrupole splitting, ΔE_Q, is very small (Figure S2; see the Experimental Section). The isomer shift $\delta = 0.43(1)$ mm s^{-1} is the same for both fits. The δ, ΔE_Q, and line width values are characteristic of ferricenium salts (e.g., $[Fe(cp^*)_2][BF_4]$, $\delta = 0.49$ mm s^{-1}, $\Delta E_Q = 0$ mm s^{-1}).[28,29] The Mössbauer spectrum shows clearly that the $[Fe^{III}(cp^*)_2]^+$ cations exist in very similar magnetic environments without significant electron-transfer delocalization between cations and anions. In comparison, ferrocene species such as $Fe^{II}(cp^*)_2$ exhibit $\Delta E_Q \approx 2.3$ mm s^{-1}.[29]

The Mössbauer and EPR data are consistent with all five $[Fe^{III}(cp^*)_2]^+$ cations occupying similar environments. Cation−cation and cation−anion electron-transfer interactions are not significant.

Magnetic Susceptibility Studies on $[Fe(cp^*)_2]_5[HS_2Mo_{18}O_{62}]\cdot 3DMF\cdot 2Et_2O$. Details of the diamagnetic and other corrections for this high molar mass species are given in the Experimental Section. When diamagnetic corrections for all atoms are taken into account, the μ_{eff} and χ_m^{-1} data show a gradual but small curvature downward between 4 and 300 K. Thus, the complex displays a deviation from linear Curie−Weiss ($\chi = C/(T - \Theta)$) behavior. The corresponding μ_{eff} values decrease gradually from 5.79 μ_B at 300 K to 5.02 μ_B at 4.2 K. If μ_{eff} per $[Fe^{III}(cp^*)_2]^+$ cation values are presented (the format used by Le Maguerés et al.),[18] they correspond to 2.59 μ_B (300 K) and 2.24 μ_B (4.2 K). It is common in studies of polyoxometalate magnetism to allow for a significant TIP term associated with the presence of the Mo^{VI} (d^0) centers.[18] The TIP term for $[Fe(cp^*)_2]_5[HS_2Mo_{18}O_{62}]\cdot 3DMF\cdot 2Et_2O$ was estimated by undertaking a linear regression fitting of the χ_m vs $1/T$ data and gave a value of 1450×10^{-6} cm^3 mol^{-1} from the y-axis intercept. The TIP-corrected data are shown in Figure 4. The recalculated μ_{eff} value is now seen to be 5.48 μ_B and independent of temperature in the range of 300−100 K. At lower temperatures, a gradual decrease occurs until a value of 5.02 μ_B is obtained at 4.2 K. If the μ_{eff} per $[Fe^{III}(cp^*)_2]^+$ cation values are considered, the temperature dependence and sizes of μ_{eff} are similar to those reported previously for related Keggin species.[18] Thus, for $[Fe(cp^*)_2]_5[HS_2Mo_{18}O_{62}]\cdot 3DMF\cdot 2Et_2O$ and $[Fe(cp^*)_2]_4[SiMo_{12}O_{40}]\cdot DMF$, the respective values at 300 K are $\mu_{eff} = 2.45$ and 2.49 μ_B (per $[Fe^{III}(cp^*)_2]^+$); the Curie−Weiss constant $\Theta = -1$ and −1.9 K.

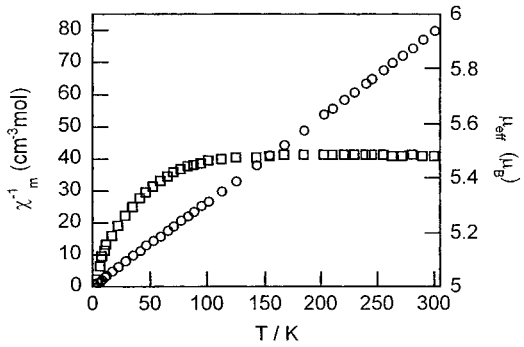

Figure 4. μ_{eff} (□) and χ_m^{-1} (○) vs temperature magnetic data for powdered $[Fe(cp^*)_2]_5[HS_2Mo_{18}O_{62}]\cdot 3DMF\cdot 2Et_2O$ corrected for a TIP susceptibility contribution of 1450×10^{-6} cm^3 mol^{-1}. The field value is 10000 G.

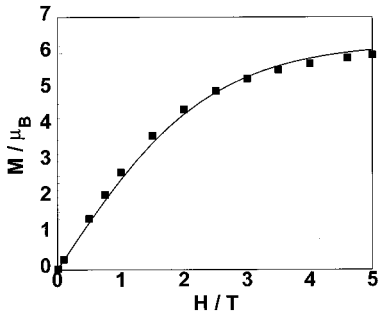

Figure 5. Magnetization isotherm for $[Fe(cp^*)_2]_5[HS_2Mo_{18}O_{62}]\cdot 3DMF\cdot 2Et_2O$ at 2 K corrected for TIP susceptibility. The solid line represents the best fit using a Brillouin model with $g = 2.51$ for five $S = 1/2$ centers.

The gradual decrease in μ_{eff} found at temperatures below 100 K is expected for a distorted low-spin Fe^{III} (d^5) system of the $[Fe^{III}(cp^*)_2]^+$ type.[5] These data confirm that any magnetic interactions between atoms or cations and anions in $[Fe(cp^*)_2]_5[HS_2Mo_{18}O_{62}]\cdot 3DMF\cdot 2Et_2O$ are extremely weak. Further confirmation of this was obtained from high-field magnetization isotherms measured on the present compound.

In Figure 5 it can be seen that the 2 K data do not saturate at the highest available field, 5 T, and have $M \approx 6$ Nμ_B indicative of five $S = 1/2$ centers with $g > 2$. The

(25) Quagliano, J. V.; Fujita, J.; Franz, G.; Phillips, D. J.; Wamsley, J. A.; Tyree, S. Y. *J. Am. Chem. Soc.* **1961**, *83*, 3770−3773.
(26) Sutton, G. J. *J. Aust. Chem.* **1967**, *20*, 1859−1863.
(27) Young, J. F.; Gillard, R. D.; Wilkinson, G. *J. Chem. Soc.* **1964**, 5176−5189.
(28) Morrison, W. H.; Hendrickson, D. N., Jr. *Inorg. Chem.* **1975**, *14*, 2331−2346.
(29) Birchall, T.; Drummond, I. *Inorg. Chem.* **1971**, *10*, 399−401.

Table 3. Comparison of Bond Distances (Å) in $(Et_4N)_4[S_2Mo_{18}O_{62}]$, $(NBu_4)_5[HS_2Mo_{18}O_{62}]$, and $(NBu_4)_5H_3S_2Mo_{18}O_{62}]\cdot 4MeCN$ (Mean Values in Brackets)

		$[S_2Mo_{18}O_{62}]^{4-}$ (295 K)[c]	$[HS_2Mo_{18}O_{62}]^{5-}$ (173K)[d]	$[H_3S_2Mo_{18}O_{62}]^{5-}$ (170 K)[e]
Mo···Mo_e[a]	within triplets	3.422(3)−3.444(3) [3.436]	3.449(1)−3.455(1) [3.447]	3.432(1)−3.461(1) [3.450]
	within belts	3.438(3)−3.456(3) [3.448]	3.443(1)−3.459(1) [3.452]	3.447(1)−3.461(1) [3.455]
Mo···Mo_c[a]	within belts	3.685(3)−3.700(3) [3.693]	3.696(1)−3.713(1) [3.704]	3.747(1)−3.767(1) [3.759]
	between belts and triplets	3.681(3)−3.785(3) [3.737]	3.704(1)−3.795(1) [3.744]	3.726(1)−3.836(1) [3.772]
	between belts	3.791(3)−3.805(3) [3.801]	3.756(1)−3.801(1) [3.780]	3.732(1)−3.743(1) [3.736]
Mo···S	axial	3.586(5)−3.593(4) [3.595]	3.580(2)−3.603(2) [3.660]	3.582(1)−3.602(1) [3.590]
	lateral	3.514(5)−3.599(5) [3.569]	3.551(2)−3.603(2) [3.573]	3.597(1)−3.639(1) [3.609]
S···S		3.918(7)	3.933(3)	3.922(1)
S−O		1.42(1)−1.52(1) [1.471]	1.463(4), 1.464(4), 1.466(4), 1.494(4)	1.461(3)−1.498(1) [1.473]
Mo−O(S)	axial	2.43−2.53 [2.47]	2.483(4)−2.496(4) [2.491]	2.473(3)−2.495(4) [2.485]
	lateral		2.444(4)−2.505(4) [2.480]	2.487(3)−2.531(4) [2.507]
Mo−O_t		1.62(1)−1.69(1) [1.659]	1.667(4)−1.689(4) [1.681]	1.674(4)−1.689(5) [1.683]
Mo−O_e	within triplets			
	"short"	[1.827]	1.853(4)−1.885(4) [1.871]	1.906(4)−1.929(4) [1.914]
	"long"	[2.000]	1.980(4)−1.983(4) [1.982]	1.917(4)−1.966(4) [1.947]
	within belts[b]	[1.872], [1.945]	1.883(4)−1.926(4) [1.902]	1.895(4)−1.913(4) [1.930]
Mo−O_c	within belts[b]	[1.867], [1.933]	1.882(4)−1.918(4) [1.897]	1.915(4)−1.934(4) [1.924]
	triplets−belts[b]	[1.798], [2.015]	1.805(4)−2.071(4) [1.933]	
	belts−belts[b]	[1.792], [2.045]	1.807(4)−2.031(4) [1.906]	1.868(4)−1.892(4) [1.882]

[a] Mo_c and O_c denote distances in corner-sharing octahedra and Mo_e and O_e in edge-sharing octahedra. [b] Mean values for short and long bonds, respectively. [c] Reference 8. [d] This work. [e] Reference 16.

magnetization data fitted well to a Brillouin function calculated for the summation of five independent $S = 1/2$ centers, the plot for the 2 K data being given in Figure 5. The best-fit g value of 2.51 compares well with that deduced from the EPR spectrum, 2.49, and with those for related $[FeCp^*_2]^+$ salts of polyoxometalates.[18] The other magnetization isotherms determined at 3, 4, 5.5, 7, and 10 K likewise gave good fits to this model but with slightly larger g values required, viz., 2.59 at 4 K and 2.73 at 10 K. This temperature variation in g most probably reflects the need for the magnetization to be calculated using a $^2T_{2g}$ (split) state and the observed g_{11} and g_1 values, rather than using a simple Brillouin $S = 1/2$ model. Nevertheless, the magnetization data support the lack of interaction between $[Fecp^*_2]^+$ cations and between $[Fecp^*_2]^+$ and $[HS_2Mo_{18}O_{62}]^{5-}$.

In summary, the total spectroscopic and magnetic data indicate that $[Fe(cp^*)_2]_5[HS_2Mo_{18}O_{62}]\cdot 3DMF\cdot 2Et_2O$ features five magnetically independent decamethylferricenium cations and an EPR-silent, (2 e^-)-reduced $[HS_2Mo_{18}O_{62}]$ anion which provides a TIP susceptibility contribution of 1450×10^{-6} $cm^3\ mol^{-1}$. Its crystal structure could not be obtained, but that of the NBu_4^+ salt is now described.

Crystal Structure of $[NBu_4]_5[HS_2Mo_{18}O_{62}]\cdot 2H_2O$ and Comparison to Related Anions in Various Redox States. While small crystals of $[Fe(cp^*)_2]_5[HS_2Mo_{18}O_{62}]\cdot 3DMF\cdot 2Et_2O$ could be grown, they were not suitable for X-ray analysis. However, $[NBu_4]_5[HS_2Mo_{18}O_{62}]\cdot 2H_2O$ was crystallized from (wet) MeCN, into which Et_2O was diffused, and this proved suitable for crystallographic study. The space group is $C2/c$ with four formula units, the unit cell containing 20 $[NBu_4]^+$ cations. Two H_2O solvent molecules were found but no MeCN solvent molecules. On the basis of the analytical data, one proton is included for electroneutrality. Figure 6 is an ORTEP representation of the anion structure and provides a numbering scheme.

The (4 e^-, 3 H^+)-reduced salt $[NBu_4]_5[H_3S_2Mo_{18}O_{62}]\cdot 4MeCN$ also crystallizes in $C2/c$ with four formula units and features five NBu_4^+ cations per anion.[16] However, 16 MeCN molecules of crystallization were present in the unit cell. The structure of the anion in $[NEt_4]_4[S_2Mo_{18}O_{62}]\cdot MeCN$ can now be compared with those of the (2 e^-, 1 H^+)- and (4 e^-, 3 H^+)-reduced anions as they exist in $[NBu_4]_5[HS_2Mo_{18}O_{62}]\cdot 2H_2O$ and $[NBu_4]_5[H_3S_2Mo_{18}O_{62}]\cdot 4MeCN$, respectively.[8,16] The former was determined at 295 K and the latter at 173 and 170 K. A comparison of interatomic distances is given in Table 3. Each anion is present as the α-Dawson isomer with nominal point D_{3h} symmetry.

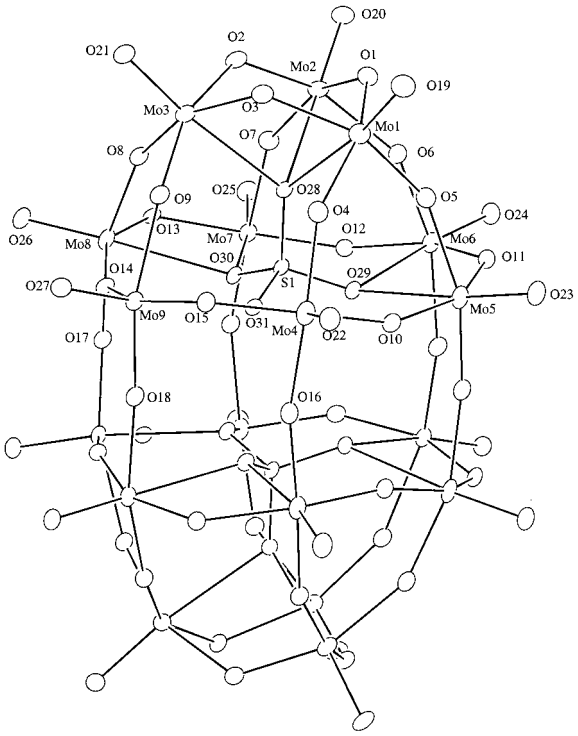

Figure 6. Structure of $[NBu_4]_5[HS_2Mo_{18}O_{62}]\cdot 2H_2O$ displaying atomic labeling and the vibrational ellipsoid (50% probability).

The anion expands significantly with the addition of two and then four electrons. Compared to the oxidized form, the largest structural differences are seen in the two equatorial

belts of six edge- and corner-sharing MoO_6 octahedra (Table 3). The following main points emerge from the structures.

(i) The average Mo···Mo distances between the corner-sharing MoO_6 octahedra in the belts increase in the order 3.693, 3.704, and 3.759 Å for the oxidized, (2 e^-, 1 H^+)-reduced, and (4 e^-, 3 H^+)-reduced anions. The equivalent distances between the edge-sharing MoO_6 octahedra remain constant, close to 3.45 Å.

(ii) The Mo−O (bridging) distances within the belts alternate significantly in the oxidized form but less so in the two reduced forms. This feature is also seen within the trinuclear caps of edge-sharing MoO_6 octahedra: oxidized, av 1.827 and 2.000 Å; (2 e^-, 1 H^+)-reduced, 1.871 and 1.982 Å; (4 e^-, 3 H^+)-reduced, 1.914 and 1.947 Å.

(iii) The Mo···Mo distances along the bonds which connect the two belts *decrease* in the order 3.801, 3.780, and 3.736 Å, making these distances the shortest for the three inequivalent sets of corner-sharing octahedra in each anion. This is consistent with the two or four added electrons localizing essentially in molecular orbitals which are bonding with respect to interactions between the belts. Symmetry-equivalent octahedra share a single bridging oxo ligand, and the arrangement correlates with the known stability of spin-paired $[Mo^{V}O]_2(\mu\text{-}O)$ fragments in Mo(V) chemistry.[30] Longer range coupling contributions are probable, as indicated by spectroscopic and magnetic investigations of other reduced Dawson anions.[31−34]

(iv) The Mo···Mo distances along the bridges between the caps and the belts increase on average in the order 3.737, 3.744, and 3.772 Å. The observed spread of values around each of these averages (Table 3) is caused by a pronounced puckering in the belts in the oxidized anion, but in the two reduced anions, a rotation of the caps relative to the belts is present as well.

(v) For the Mo−O−Mo bridges between the caps and the belts, this puckering in the oxidized form leads to alternating shorter and longer Mo−O bonds ($\Delta = 0.217$ Å) originating in the belts. This is less pronounced in the (2 e^-, 1 H^+)-reduced form ($\Delta = 0.142$ Å). However, in the (4 e^-, 3 H^+)-reduced anion, all Mo−O bonds originating in the central belts are longer than those originating at the caps. This is proposed to be consistent with the added electrons localizing in those belts.[16] In addition, the longest of these bonds were suggested to be the sites of protonation. An alternative view is that the pattern is a vestige of the puckering discussed above. Certainly, sites of protonation in the (2 e^-, 1 H^+)-reduced form cannot be discerned from the data reported here.

(vi) The (2 e^-, 1 H^+)-reduced species $[NBu_4]_5[HS_2Mo_{18}O_{62}]\cdot 2H_2O$ displays the α-Dawson structure. Solution electrochemical studies reported above confirm that the anion derived from $[Fe(cp^*)_2]_5[HS_2Mo_{18}O_{62}]\cdot 3DMF\cdot 2Et_2O$ is at the same redox and protonation state.

Acknowledgment. Financial support from the Australian Research Council is gratefully acknowledged.

Supporting Information Available: Tables S1−S4 (X-ray crystallographic data related to atomic coordinates, anisotropic displacement parameters, intramolecular distances, and intramolecular bond angles) and S5 (conductivity data), Figures S1 (ESR spectrum) and S2 (Mössbauer spectrum) and an X-ray crystallographic file for α- $[NBu_4]_5[HS_2Mo_{18}O_{62}]\cdot 2H_2O$ in CIF format. This material is available free of charge via the Internet at http://pubs.acs.org.

IC010780S

(30) Hendrickson, D. N.; Sohn, Y. S.; Gray, H. B. *Inorg. Chem.* **1971**, *10*, 1559−1563.
(31) Steifel, E. I. *Prog. Inorg. Chem.* **1977**, *22*, 1−223.
(32) Kazanskii, L. P.; Fedotov, M. A. *J. Chem. Soc., Chem. Commun.* **1980**, 644−646.
(33) Kozik, M.; Hammer, C. F.; Baker, L. C. W. *J. Am. Chem. Soc.* **1986**, *108*, 2748−2749.
(34) Casan-Pastor, N.; Baker, L. C. W. *J. Am. Chem. Soc.* **1992**, *114*, 10384−10394.